Carrier wave effect in nonresonant inelastic scanning tunneling spectroscopy of molecules with delocalized frontier orbitals

Antti Korventausta*
Department of Physics, Tampere University of Technology, P.O. Box 692, FIN-33101 Tampere, Finland

Jörg Meyer
Institut für Festkörperphysik, Abteilung Atomare und Molekulare Strukturen (ATMOS), Leibniz Universität Hannover, Appelstrasse 2, 30167 Hannover, Germany

Jouko Nieminen
Department of Physics, Tampere University of Technology, P.O. Box 692, FIN-33101 Tampere, Finland
(Received 18 December 2009; revised manuscript received 19 May 2010; published 21 June 2010)

In this work we present a method for simulating the electron-vibration coupling in adsorbate molecules using a tight-binding formalism for the electronic degrees of freedom and a real-space description of the molecular vibrations. First, we derive a formalism which is very transparent in recognizing the effect of a local vibrational perturbation on the local electronic structure at any location. Second, we apply the method to nonresonant inelastic electron-tunneling spectroscopy (IETS) of two sample molecules on generic model substrates as typically accessible within a scanning tunneling microscopy (STM) experiment. The foremost observation is that the intensity of the STM-IETS signal is not necessarily strongest in the spatial vicinity of the vibrational perturbation. Instead, it is dependent on the delocalization of the molecular orbitals, which may lead to a strong intensity quite far from the vibration. Since this is an effect of the electronic structure and not related to the transfer of the vibrational motion itself, the molecular orbitals can be treated as "carrier waves" of the signal from a vibrational perturbation. This effect may be important in determining the orientation of an adsorbed molecule on a substrate surface or in manipulating adsorbed molecules with an STM tip.

DOI: 10.1103/PhysRevB.81.245426 PACS number(s): 68.37.Ef, 68.43.Pq, 82.37.Gk

I. INTRODUCTION

Application of scanning tunneling microscopy to inelastic electron-tunneling spectroscopy (STM-IETS) in small molecular adsorbate systems has attracted a lot of activity recently.[1–5] Good spatial resolution has made it possible to measure d^2I/dV^2 spectra at a chosen position above the adsorbate molecule, or even make a topographic map of vibrational modifications to the local electronic structure. Interestingly, the STM-IETS signal for localized molecular vibrations can be observed quite far away from the spatial location of a chosen vibration mode.[6,7] Since the interpretation of d^2I/dV^2 spectra and corresponding topographic maps is far less obvious than scanning tunneling spectra (STS) and dI/dV maps, it is obvious that computational methods with a strong interpretational ability are required.

The best known theoretical approach to analyzing and predicting STM-IETS results is the standard Tersoff-Hamann approach[8] as generalized to take electron-vibration coupling into account.[9,10] In order to improve recognition of different modes, symmetry selection rules have been incorporated into this theory by Lorente *et al.*[11] The transparency of theoretical calculations can be taken a step further by utilizing Green's-function methods in an atomic- or molecular-orbital basis. Especially the formalism independently derived by Todorov[12] and Pendry[13] has proven very useful in decomposing the tunneling signal into tunneling channels,[14] and there is no restriction against applying channel analysis to inelastic tunneling. Inelastic effects have been incorporated into STS calculations at least in connection with high-temperature superconductivity.[15]

In the following, we consider inelastic tunneling in the framework of tunneling channels and paths,[16] especially intramolecular paths. This is possible in the case of delocalized frontier orbitals (FOs), if they are not too strongly mixed with the substrate wave functions. In principle, this decoupling of the adsorbate from the substrate would require either adsorption on an insulating layer or physisorption on a metal surface. This work is very much inspired by the experiments described in the supporting material included with Ref. 4 on meta-dichlorobenzene (MDCB) molecules on Au(111), where the vibrational signal strongly depends on the position of the tip.

In order to get generic and transparent results, we apply model substrates with either constant or Lorentzian density of states, which couples to the electronic structure of the molecule in the form of a self-energy. As examples, we consider two substituted benzene molecules: chlorobenzene (CB) and MDCB. Because their frontier molecular orbitals are of π type, the vibrational modes of these molecules are modeled with bosonic couplings to the p_z orbitals of the chlorine atoms and the adjoining carbon atoms.

Although we attempt to keep this study generic, we choose these two molecules due to their symmetry and favorable frontier orbitals for demonstrational purposes. First, the molecules are rather simple and survive adsorption onto a noble-metal surface without considerable structural changes. Second, some of the vibrational modes can be characterized mainly by stretching and/or bending of carbon-chlorine bonds, which simplifies the analysis of motion in the local basis where electronic degrees of freedom are described in

tight-binding formalism and molecular vibrations are considered in terms of real-space motion.

The present study is restricted to *nonresonant tunneling* through an adsorbate molecule with a relatively wide gap between the states which are (energetically) close to the highest occupied and lowest unoccupied molecular orbitals (HOMOs and LUMOs, respectively). Hence, the tunneling takes place through a tail of the surface wave functions only slightly mixing with those so-called frontier orbitals. Since the vibrational energies are very small as compared to the gap in the electronic spectrum, the vibrations open an *inelastic channel* through the molecule, which will be shown in the following sections. It is crucial in this case that the local density of states (LDOS) around Fermi energy varies only moderately as a function of energy, and thus the fingerprints of vibrational excitations are simple to recognize. There are also two essential assumptions done: first, the vibrational modes are local, i.e., they can be clearly attributed to the motion of a finite group of atoms. Second, the frontier orbitals are delocalized. In such a case, we expect that the signal from a localized vibrational mode is strongly spatially extended.

Within this framework, we show that electronic orbitals act as *carrier waves* for a vibrational signal, i.e., the observation of this signal at a certain position does not necessarily mean that the vibration itself is extended to the site of observation. Furthermore, we find a strong nontrivial spatial dependence of the observed IETS signal. This effect may be helpful in determining the adsorption geometry of molecules, whose internal structure may be difficult to resolve from a topographic STM image.

II. THEORY

We model inelastic tunneling through the chosen molecules by utilizing the *equilibrium* Green's-function description of the molecule-substrate system and the vibrational modes. Although transport calculations concerning nanostructures between metallic leads should, in general, be performed using nonequilibrium Green's function methods, it is still very much the state of the art in STM and STS calculations to equate the differential conductance to the local density of states of the sample at the position of the tip. This entity, on the other hand, is related to the equilibrium Green's function of the system. Although our formulation of the STS spectrum differs from, for example, the standard Tersoff-Hamann approach,[8] the applied equations fall into the same category of equilibrium calculations.

In this section, we present our theory before its numerical evaluation in the next section as follows: first, we construct the Green's function of a free molecule in the tight-binding basis in Sec. II A and derive generic self-energy formulas for both the substrate and electron-vibration coupling (Secs. II A 1 and II A 2, respectively). Then, in Sec. II B, we discuss the relation between Green's function in tight-binding basis and the Todorov-Pendry (TP) tunneling equation.[12,13] TP approach can be rephrased in terms of spectral terms including matrix elements of retarded and advanced Green's function and the imaginary part of the total self-energy, which formally is similar to the *nonequilibrium* Landauer-Büttiker approach as formulated by Meir and Wingreen.[17] Although we consider the equilibrium Green's-function limit, this representation is able to expose the matrix elements of the density matrix explicitly for further tunneling channel analysis. This relation between the approaches provides a fairly straightforward way to include vibrational modes, as employed in our recent STS analysis of high-temperature superconductors.[15] The equations derived here, on the other hand, are generalizations of the elastic and inelastic terms by Lorente and Persson.[10]

A. Constructing the molecular Green's function

Let us start with a Hamiltonian H_0 for a free molecule, which is diagonal in the molecular-orbital basis. As discussed in Ref. 14, the Green's function in an atomic-orbital basis $G_{\alpha\beta}$ can be written using the energies and linear combination coefficients of molecular orbitals,

$$G^0_{\alpha\beta}(E) = \sum_\mu \langle\alpha|\mu\rangle G^0_{\mu\mu}(E)\langle\mu|\beta\rangle = \sum_\mu \frac{c^*_\alpha(\mu)c_\beta(\mu)}{E - E_\mu + i\eta}. \quad (1)$$

Here we used molecular orbitals $|\mu\rangle$ with energies E_μ such that

$$H_0|\mu\rangle = E_\mu|\mu\rangle$$

and their expansion into atomic orbitals with expansion coefficients $c_\alpha(\mu)$ $|\alpha\rangle$

$$|\mu\rangle = \sum_\alpha |\alpha\rangle\langle\alpha|\mu\rangle = \sum_\alpha c_\alpha(\mu)|\alpha\rangle.$$

The Green's function of an unperturbed molecule can be coupled to a substrate Green's function and molecular vibrations by utilizing Dyson's equation. If we concentrate on the Green's function of the coupled molecule, an appropriate way to include substrate and vibrations is to write self-energy matrices for both of them,

$$\Sigma_{\alpha\beta} = \Sigma^{a-s}_{\alpha\beta} + \Sigma^{e-v}_{\alpha\beta}, \quad (2)$$

Σ^{a-s} is used to model the adsorbate substrate and Σ^{e-v} refers to the electron-vibration coupling. Unless otherwise indicated by a superscript, G and Σ refer to retarded Green's Functions and self-energies, respectively. We will discuss the form of the terms in Secs. II A 1 and II A 2, respectively. Here we notice that self-energy terms can serve at least two purposes: first, the system is divided into several regions—such as tip, adsorbate, and substrate—one can concentrate on a chosen region (adsorbate) by modeling the rest of the system by a self-energy matrix. Second, many-body effects, such as electronic excitations or electron-boson couplings can be effectively taken as a term shifting and broadening, i.e., dressing eigenstates of the electrons of the noninteracting system.

The effect of the self-energy terms can be incorporated to the Green's function in a standard way by solving the Dyson's equation,

$$G = G^0 + G^0\Sigma G = G^0 + G^0 T G^0, \tag{3}$$

where T is the transition matrix. A clever way to obtain the exact solution and keep track on the effects of distinct elements of self-energy is to express the self-energy as a sum of 1×1 diagonal blocks and 2×2 blocks with zeros in the diagonal. It is simple to derive the corresponding T matrix for each block and apply Dyson's equation successively,

$$G^{n+1}_{\alpha\beta} = G^n_{\alpha\beta} + G^n_{\alpha i} T^n_{ij} G^n_{j\beta}, \tag{4}$$

where T^n_{ij} is a functional of the Green's function G^n of the nth step and the chosen self-energy block Σ_{ij} of the present step. Note that i and j run over all the orbital pairs of the system. The idea of this algorithm is originally presented in Ref. 18.

First, let us consider the transition matrix corresponding to a 1×1 diagonal block Σ_{ii} and the corresponding T matrix to derive G^{n+1} from G^n. It is easy to see that a single term leads to the expression,

$$T^n_{ii} = \frac{\Sigma_{ii}}{1 - \Sigma_{ii} G^n_{ii}}. \tag{5}$$

Second, let us look at 2×2 blocks of the form

$$\Sigma = \begin{pmatrix} 0 & \Sigma_{ij} \\ \Sigma_{ji} & 0 \end{pmatrix}.$$

The corresponding transfer matrix is (see Ref. 18)

$$T^n_{ij} = \frac{1}{Det}\begin{pmatrix} \Sigma_{ij} G^n_{jj} \Sigma_{ji} & \Sigma_{ij}(1 - G^n_{ij}\Sigma_{ji}) \\ \Sigma_{ji}(1 - G^n_{ji}\Sigma_{ij}) & \Sigma_{ji} G^n_{ii} \Sigma_{ij} \end{pmatrix}, \tag{6}$$

where $Det = (1 - G^n_{ij}\Sigma_{ji})(1 - G^n_{ji}\Sigma_{ij}) - \Sigma_{ji} G^n_{ii} \Sigma_{ij} G^n_{jj}$.

As an example, let us look at the effect of a perturbation by a term T_{ij} to an arbitrary off-diagonal element between orbitals $|\alpha\rangle$ and $|\beta\rangle$. From Dyson's equation, one can readily extract the change in the Green's function due to the self-energy

$$\Delta G_{\alpha\beta}(E) = G^0_{\alpha,1} T_{ij} G^0_{1,\beta} = \sum_{\mu,\nu} \frac{c^*_\alpha(\mu) c_\beta(\nu) c^*_1(\nu) c_1(\mu) T_{ij}}{(E - E_\mu + i\eta)(E - E_\nu + i\eta)}. \tag{7}$$

Since this determines the change in the elements of the density matrix, $\Delta\rho_{\alpha\beta} = -\frac{1}{\pi}\Im(\Delta G_{\alpha\beta})$, it is straightforward from Eq. (7) to make a partition into an elastic part

$$\Delta\rho^{el}_{\alpha\beta} = \rho^0_{\alpha i}\Re(T_{ij} G^0_{j\beta}) + \Re(G^0_{\alpha i} T_{ij})\rho^0_{j\beta} \tag{8}$$

and inelastic part

$$\Delta\rho^{inel}_{\alpha\beta} = -\frac{1}{\pi}\Re(G^0_{\alpha i} G^{0*}_{j\beta})\Im(T_{ij}), \tag{9}$$

which is an obvious generalization of the formulation of Lorente and Persson in Ref. 10. It should be noted that within the gap, the density of states is very low and thus the corresponding tunneling channel is essentially inelastic.

In the case of nonresonant tunneling in the neighborhood of the Fermi energy, it can be assumed that $|E - E_\mu| \gg 0$. Hence, the change in the density matrix due to the perturbation can be written approximately

$$\Delta\rho_{\alpha\beta}(E) = -\frac{1}{\pi}\Re(G^0_{\alpha i} G^{0*}_{j\beta})\Im(T_{ij}) \approx \Im(T_{ij}) \sum_{\mu,\nu} \frac{c^*_\alpha(\mu) c_i(\mu) c^*_\beta(\nu) c_j(\nu)}{(E - E_\mu)(E - E_\nu)}. \tag{10}$$

Considering Eq. (5), we notice that $T_{ii} \approx \Sigma_{ii}$ in the neighborhood of E_F since $G(E)$ is small at energies far from the eigenstates E_μ. Therefore, the possible kinks to the LDOS result from discontinuities typical to the imaginary part of the self-energy. This means that the kinks coincide rather accurately with the vibrational mode energies. Since the IETS signal is proportional to the derivative of the LDOS (or the density matrix), these kinks are seen as peaks in experiments. In reality, however, the steps are smoothened since the molecular vibrations couple to the surface phonons. In addition, the wave functions of the substrate interact with the molecular orbital and therefore the imaginary part of $G_{\alpha\alpha}$ is not necessarily zero.

1. Self-energy model of the substrate

The molecule-substrate self-energy is written in the standard way (the term "contact self-energy" is used, see, e.g., Refs. 19 and 20),

$$\Sigma^{a-s}_{\alpha\beta} = V_{\alpha s} G^0_{ss'} V_{s'\beta}, \tag{11}$$

where $G_{ss'}$ is the Green's function for the substrate. In general, the matrix elements of the substrate Green's function can be calculated from the density matrix $\rho_{ss'}$, whose diagonal elements give the local density of states,

$$G^0_{ss'}(E) = \int \frac{\rho_{ss'}(E')}{E - E' + i\eta} dE'. \tag{12}$$

This relation could, in principle, be used to include any kind of electronic structure of the surface to tunneling simulations. In order to keep the computations transparent, we reduce the substrate to as simple a form as possible and assume a diagonal self-energy with a constant coupling $V_{\alpha s}$ to the p_z atomic orbitals of the adsorbate molecule.

If we assume a constant LDOS for the substrate with finite band width W and construct the full self-energy with the Kramers-Kronig transformation. The final form of the self-energy is

$$\Sigma^{a-s}_{\alpha\alpha}(E) = -\frac{|V_{\alpha s}|^2}{2\pi W}\ln\left(\frac{E - E_s + i\eta - W}{E - E_s + i\eta + W}\right). \tag{13}$$

Another simple approximation is the narrow Lorentzian band,

$$\Sigma^{a-s}_{\alpha\alpha}(E) = |V_{\alpha s}|^2 \frac{1}{E - E_s + iW}. \tag{14}$$

These two examples can be used (with different widths) to model two extreme examples of (1) a wide-band substrate and (2) a substrate with localized states at the surface.

2. Electron-vibration self-energy

While constructing the Green's function for electrons is relatively straightforward, an exhaustive modeling of the

electron-vibration coupling is much more elaborate. There may be several vibrational modes, whose coupling to electronic degrees of freedom is strongly selective due to symmetry. In addition to such symmetry considerations, the density of vibrational modes is needed in order to derive the appropriate self-energy terms. As soon as this difficult part of the problem is solved, one can straightforwardly apply Dyson's equation to calculate the perturbation of the electronic structure by the molecular vibrations. The appearance of the perturbation at a chosen position is, in part, governed by the structure and symmetry of the molecule.

In the Appendix, we present the equations for electron-vibration self-energy, which are used in similar form quite frequently in the literature for modeling spectroscopies.[21] One feature is the explicit derivation in the atomic orbital and atomic displacement basis. In principle, it is possible to write the vibrational modes in terms of two bases. Usually, one assumes the generalized coordinate basis Q_q, which diagonalizes the vibrational Hamiltonian, and gives the eigenfrequencies Ω_q and the symmetry of each mode. However, the basis more closely related to the TB basis of electronic degrees of freedom is the one where real-space displacements of atoms are considered. In addition, we show the $T \rightarrow 0$ K limit result in tight-binding formalism, which is utilized in this study. In that limit, the self-energy is proportional to the convolution of the LDOS of the electrons and the vibrational—or in a more general case other bosonic—excitations, as shown in Eq. (A22).

For the present calculations we use some additional simplification according to the following assumptions: First, the modeled vibrational mode is localized to a certain bond between two atoms. This simplifies the vibrational density of states occurring in Eq. (A22) to $g_{IJ}(\Omega)=\delta_{IJ}\delta(\Omega-\Omega_q)$. Then we take the generic choice, where $\rho_{\delta\gamma}=-\frac{1}{\pi}\mathrm{Im}[G_{\delta\gamma}]=\delta_{\delta\gamma}\rho$, which is constant. Finally, we assume only diagonal terms $\Sigma_{\alpha\alpha}$ for electron-vibration self-energy. This is a fairly good choice for nonresonant tunneling in which case the variations are expected to be small within the range of the vibrational energy. This approximation has been widely used in spectroscopies of high-temperature superconductivity to model the effect of low energy bosonic coupling to the quasiparticles.[22]

Using these approximations in Eq. (A22), we arrive at the following functional form for the self-energy:

$$\Sigma_{\alpha\alpha}^{e-v}(E) = A\ \ln\left(\frac{\hbar\Omega_q - E - i\eta}{\hbar\Omega_q + E + i\eta}\right), \tag{15}$$

where A is a coupling coefficient, which we detail on below, and η a convergence parameter. This is the self-energy for the retarded Green's function and hence it is constructed from Eq. (A22) by performing the convolutions for positive and negative energies separately, combining these results and taking the Hilbert transformation to obtain both parts of the Green's function.

Explicit approximations similar to Eq. (15) have been used especially in modeling angular resolved photoemission spectroscopy. For example, in Ref. 21 a corresponding expression has been shown for the Debye model of phonons combined to a constant density of states of electrons.

We now discuss how the coupling coefficient A can be estimated. According to Eq. (A24) it has the form

$$A = \frac{\hbar\lambda}{2\Omega_q}\rho = \frac{\hbar}{2\Omega_q}(M_I^{\alpha\gamma})^2\rho = \frac{1}{2\Omega_q}\frac{\hbar}{m_I}\left(\frac{\partial V_{\alpha\gamma}}{\partial R_I}\right)^2\rho \tag{16}$$

with hopping integral $V_{\alpha\gamma}$ and mass m_I of the oscillating atom. For the sake of order-of-magnitude calculation, we assume that $\beta=\alpha$, $\delta=\gamma$, and $J=I$. If we consider the Slater-Koster-type scaling of tight-binding hopping integrals, they are generally of the form[23]

$$V_{\alpha\gamma} = \frac{\hbar^2}{m_e}O_{ll'm}\frac{1}{R_I^2}, \tag{17}$$

where a numerical value of $\frac{\hbar^2}{m_e}=7.62$ eV Å^2 is inserted. The parameter $O_{ll'm}$ is generally on the order of 1 but, e.g, for σ type overlap between two p orbitals, it is 3.24. The derivative with respect to the atomic distance is

$$\frac{\partial V_{\alpha\gamma}}{\partial R_I} = -\frac{2}{R_I}V_{\alpha\gamma}. \tag{18}$$

With atomic mass in atomic units, $m_I=\mu u$, we end up with

$$A = \frac{\hbar}{2\Omega_q}\frac{4}{\mu u R_I^2}V_{\alpha\gamma}^2\rho = \frac{\hbar^2}{u}\frac{1}{\hbar\Omega_q}\frac{2}{\mu R_I^2}V_{\alpha\gamma}^2\rho, \tag{19}$$

where $\frac{\hbar^2}{u}=4.18$ meV Å^2 is also a useful shortcut to notice.

B. Simulation of tunneling current

To compute the tunneling spectra we apply the Todorov-Pendry expression[12,13] for the differential conductance σ between orbitals of the tip (t,t') and the sample (s,s'), which in our case yields

$$\sigma = \frac{dI}{dV} = \frac{2\pi e}{\hbar}\sum_{tt'ss'}\rho_{tt'}(E_F)V_{t's}\rho_{ss'}(E_F+eV)V_{s't}^{\dagger}. \tag{20}$$

Here the density matrix

$$\rho_{ss'} = -\frac{1}{\pi}\Im(G_{ss'}) = -\frac{1}{\pi}\sum_{\alpha}G_{s\alpha}\Im(\Sigma_{\alpha\alpha})G_{\alpha s'}^{-} \tag{21}$$

is, in fact, the spectral function written in terms of the retarded/advanced Green's functions and the self-energy.[24] The latter formalism leads to the equilibrium Green's-function limit of the Landauer-Büttiker approach, analogous to formulation by Meir and Wingreen.[17,20]

Equation (20) differs from the more commonly used Tersoff-Hamann approach[8] in that it takes—in its general form—into account the details of the symmetry of the tip orbitals and their overlap with the surface orbitals. In this work, we also use a simplified version of Eq. (20), which assumes that the tip probes only one atomic orbital of the molecule at a time. Hence, we take $\frac{dI}{dV}(r)\propto\rho(r)$, where $\rho(r)=\langle r|\alpha\rangle\rho_{\alpha\beta}\langle\beta|r\rangle$. Or if we simply look at the matrix element of the partial differential conductance, it is sufficient to consider the term

TABLE I. The linear combination coefficients of carbon p_z orbitals for the frontier orbitals of benzene. The even MOs are denoted by "g" and the odd MOs are denoted by "u."

p orbital	HOMO(g)	HOMO(u)	LUMO(u)	LUMO(g)
1	−1.00	0.00	0.00	−1.00
2 (6)	−0.50	−(+)1.00	+(−)0.50	0.50
3 (5)	0.50	−(+)1.00	−(+)0.50	0.50
4	1.00	0.00	0.00	−1.00

$$\left[\frac{dI}{dV}(V_b)\right]_{\alpha\beta} \propto \rho_{\alpha\beta}(E_F + eV_b). \tag{22}$$

Furthermore, the partial IETS signal is approximated by simply taking a derivative of the differential conductance with respect to the bias voltage,

$$\left[\frac{d^2I}{dV^2}(V_b)\right]_{\alpha\beta} \propto \frac{d\rho_{\alpha\beta}}{dE}(E_F + eV_b). \tag{23}$$

Equations (22) and (23) are the two equations we use in simulating the spectra and the maps of the following sections. Since the present calculations are performed for very small bias voltages, we make a further simplification of dropping off the prefactors, since for a short energy range, the density of states of the tip can be assumed constant.

III. MODEL AND SIMULATIONAL DETAILS

A. Substituted benzene molecules

As commonly known, the C_{6h} symmetry of benzene leads to double degenerate π-type HOMOs and LUMOs. In a substituted benzene molecule, the symmetry is broken so that frontier orbitals have a defined parity. In this work, we study benzene molecules, where hydrogen atoms are replaced with chlorides forming CB and MDCB molecules, which lower the symmetry of the molecule to C_{2v}. The geometries of gas-phase CB and MDCB have been calculated based on density-functional theory with the approximation for the exchange-correlation functional due to Perdew and Wang (generalized gradient approximation-PW91) (Ref. 25) as implemented in the Vienna *ab initio* simulation program (VASP).[26] Blöchl's projector augmented wave method[27] is applied to treat the electron-ion interaction using the settings from the VASP database.[28] To decouple periodic images the structural relaxations are performed in sufficiently large simulation cells of 15 Å × 15 Å × 10 Å employing M point sampling and stopped when the forces are smaller than 0.02 eV/Å. The results agree within 0.02 Å—sufficient for the accuracy level of this study—with the results that have been obtained previously and based on which a vibrational analysis has been performed.[29,30]

The following tables show the linear combination coefficients of the atomic p_z orbitals for the FOs of an unsubstituted benzene molecule in Table I, a CB molecule in Table II, and an MDCB in Table III. The molecular orbitals have been calculated using TB, with exponential Slater-Koster hopping integrals.[31] The coefficients are used in calculating the unperturbed Green's function using Eq. (1). The numbering of the atomic orbitals is shown in Fig. 6 (right), with benzene only having the carbons (atoms 1–6), CB the carbons plus one chlorine (1–7), and MDCB having all of the atoms (1–8). The molecular-orbital calculations have been done for systems containing hydrogen 1s orbitals, and the 2s and 2p orbitals for carbon. Since the s, p_x, and p_y orbitals have negligible contributions to the π-type frontier orbitals, they are omitted.

TABLE II. The linear combination coefficients of carbon and chlorine p_z orbitals for the frontier orbitals of chlorobenzene.

p orbital	HOMO-1(u)	HOMO(g)	LUMO(g)	LUMO+1(u)
1 (3)	+(−)0.51	0.31	0.31	+(−)0.49
2	0.00	0.46	−0.59	0.01
4 (6)	−(+)0.49	−0.14	0.27	+(−)0.50
5	0.00	−0.41	−0.56	0.01
7	0.00	−0.63	0.11	0.00

Isosurfaces of the molecular orbitals for benzene, chlorobenzene, and dichlorobenzene are shown in Fig. 1, indicating how the CB and MDCB orbitals are formed from the benzene orbitals. The CB HOMO-1 orbital is clearly the benzene HOMO-1 orbital, with no contributions from the chlorine, whereas the MDCB HOMO is formed from the same orbital with large contributions from the chlorines. Similarly the CB HOMO and MDCB HOMO-1 are formed from the benzene HOMO orbital, with the chlorines contributing quite strongly. The CB LUMO+1 and MDCB LUMO orbitals are formed from the benzene LUMO, with no contribution from the chlorine in CB and slight contributions from the chlorines in MDCB. And finally the CB LUMO and MDCB LUMO+1 are formed from the benzene LUMO+1 orbital with slight contributions from the chlorine orbitals. Here one should note that the benzene MOs are degenerate and the employed naming is just to distinguish between the two different orbitals.

B. Substrate model

For a substrate, we apply both the narrow- and wide-band extremes as in Eqs. (13) and (14). In Fig. 2(a) a representative image of a wide-band self-energy is shown while (b)

TABLE III. The linear combination coefficients of carbon and chlorine p_z orbitals for the frontier orbitals of meta-dichlorobenzene.

p orbital	HOMO-1(g)	HOMO(u)	LUMO(u)	LUMO+1(g)
1	−0.55	0.00	0.00	−0.58
2 (6)	−0.28	−(+)0.34	+(−)0.50	0.31
3 (5)	0.09	−(+)0.42	−(+)0.49	0.27
4	0.24	−0.00	0.00	−0.56
7 (8)	0.48	+(−)0.45	−(+)0.10	−0.06

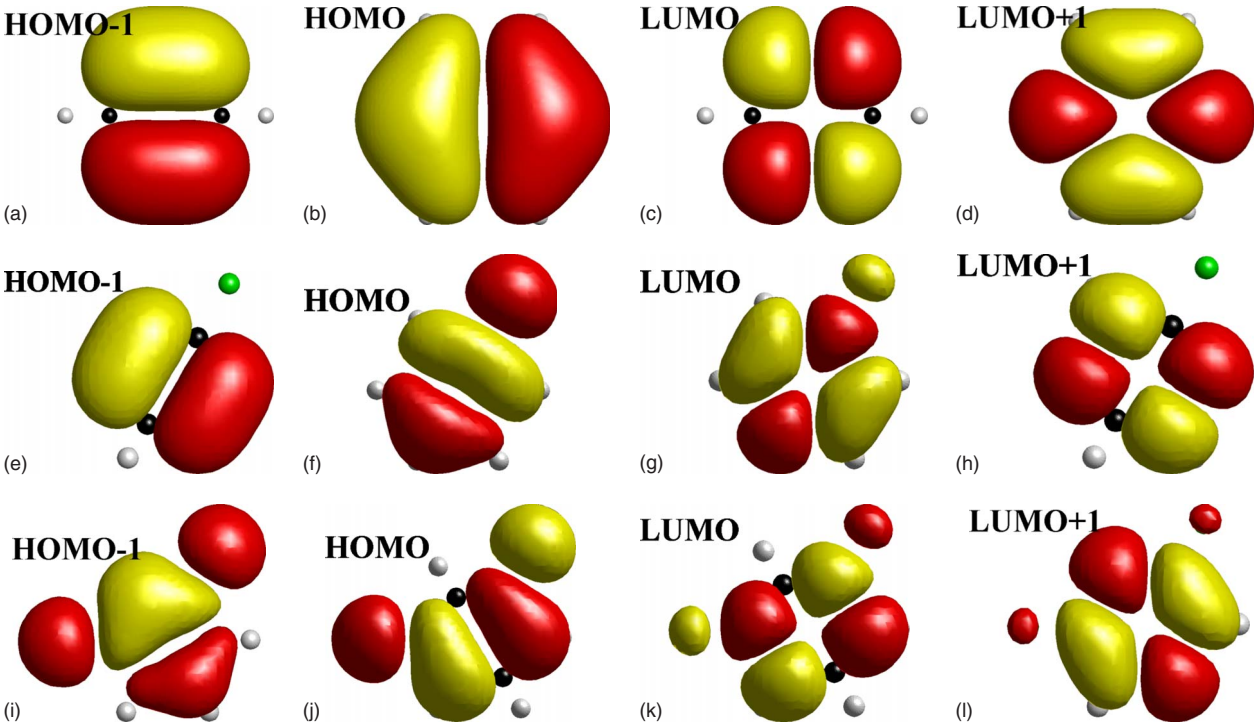

FIG. 1. (Color online) Isosurfaces of the benzene (top row), chlorobenzene (middle row), and dichlorobenzene (bottom row) molecular orbitals, showing how the frontier molecular orbitals of the molecule are constructed from atomic p_z orbitals.

depicts the Lorentzian narrow-band limit. We use substrates with both constant and Lorentzian LDOS distributions with widths of 1, 5, and 10 eV. The mean values are chosen to coincide with the Fermi energy (0 eV) and the vicinity of the HOMO (−2.5 eV) and LUMO (2.5 eV) states. The wide choice of widths is to probe the difference between the extremes of narrow- and wide-band substrates. We assume here a diagonal self-energy and a Slater-Koster[32] kind $V_{s\alpha}$ between the tip and each p_z orbital of the adsorbate molecule.

C. Vibrational modes

There is a large variety of vibrational modes for both CB and MDCB. In principle, we could derive a density matrix $g_{IJ}(\omega)$ with Eq. (A14) by summing over all the vibrational modes of the molecules. However, in this study we are trying to select specific vibrational modes related to the Cl-C bonds, and especially modes coupled to the frontier orbitals. Hence there are two issues to consider: first, the linear combination coefficients $\langle I|q\rangle$ must be significant and second, the coupling term $M_I^{\alpha\gamma}$ must be large. We are using the calculated modes from Refs. 29 and 30.

For MDCB the lowest mode with a considerable contribution from vibration of chlorine is the $A1$ symmetric mode with $\hbar\Omega_q$=24 meV. This is, however, an invisible mode since the vibration takes place mainly in a direction perpendicular to the bond. Hence, the derivative of the hopping integral between the p_z orbitals of Cl and C practically vanishes.

The next possible mode is the $A1$ symmetric mode with $\hbar\Omega_q$=48 meV. If the movement of the Cl and C atoms are projected onto the bond direction, we obtain a coefficient $\langle I|q\rangle \approx 0.30$ where the derivative is largest. Since the contribution of the corresponding part of the vibration is the square of this coefficient, and there are two bonds, the vibration of Cl in the direction of the bond gives a contribution of 0.18 of the total vibration mode, which is a relatively high value

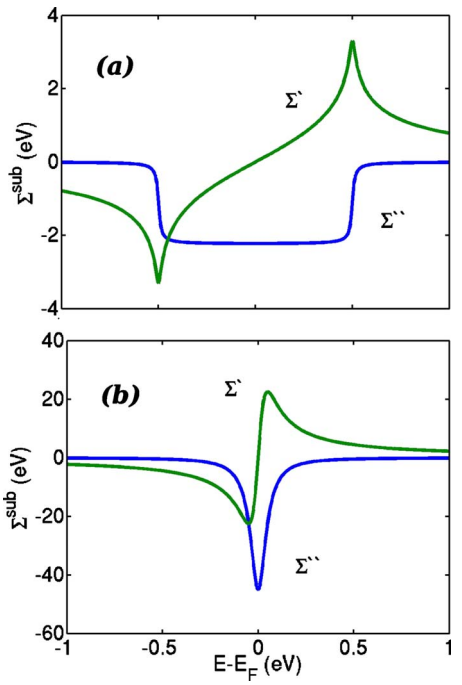

FIG. 2. (Color online) The real Σ' and imaginary Σ'' parts of the substrate self-energy for both the (a) wide-band and (b) the narrow-band examples.

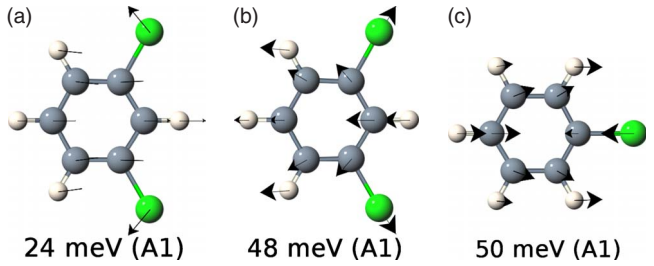

FIG. 3. (Color online) Two low-energy vibrational modes for a free MDCB molecule (left and center), and one vibrational mode for CB (right).

when compared to other modes in the neighborhood. The atomic motion of those two vibrational modes for MDCB is depicted in Fig. 3, which is taken from Ref. 30.

With similar arguments, a vibrational mode of $A1$ symmetry, with $\hbar\Omega_q=50$ meV is chosen for CB. Similarly we obtain a coefficient $\langle I|q\rangle \approx 0.31$, which is of the same size than for the mode chosen for MDCB.

For the simulations, we use these vibrational modes to create the density matrix for molecular vibrations,

$$g_{IJ}(\Omega) = \delta(\Omega - \Omega_q)|\langle I|q\rangle|^2\delta_{IJ}. \tag{24}$$

which, for simplicity, we assume diagonal as already discussed before in Sec. II A 2. To obtain the self-energy $\Sigma^{e-v}_{\alpha\alpha}(\epsilon)$ using the approximate expression (15) also discussed in that section, we choose $\mu=12$, $r=1.0$ Å, $V=1.0$ eV, and $\rho=1.0$ eV^{-1} resulting in a coupling coefficient $A \approx 13.4$ meV. In our practical calculations, we give values between 2.5 and 12.5 meV for this prefactor, mainly depending on the LDOS of the substrate at the Fermi energy. Figure 4 shows that for these parameters the imaginary part of the self-energy exhibits clear steps and the real part distinct peaks at the energy of the vibration both at positive and negative energies.

IV. RESULTS

In the following, we consider the IETS spectra of CB and MDCB molecules, and bring up the idea of a carrier wave

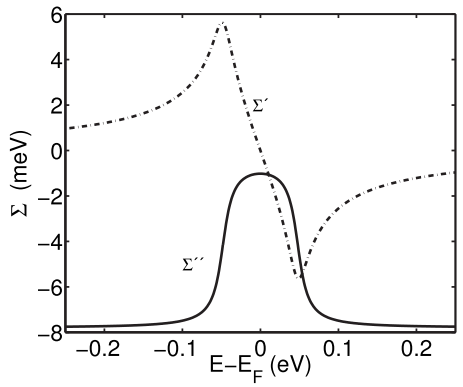

FIG. 4. Vibrational self-energy for $\Omega_q=50$ meV calculated using Eq. (A22) and Hilbert transformation. Note that the real part (Σ') shifts the states toward Fermi energy while the imaginary (Σ'') part broadens the states outside the range $-\hbar\Omega_q \rightarrow \hbar\Omega_q$.

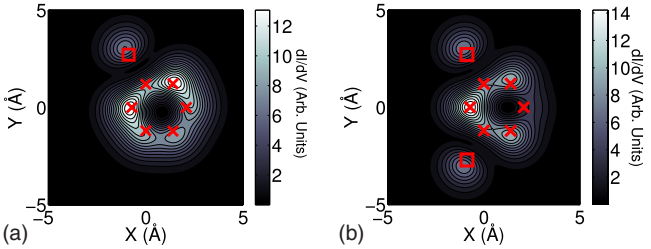

FIG. 5. (Color online) Constant height mappings of dI/dV at 2 Å above the plane of the CB (left) and MDCB (right) molecules at negative bias voltages (−48 mV for MDCB and −50 mV for CB). The substrate has been simulated using a 5 eV wide Lorentz LDOS distribution centered around the Fermi energy. The carbon atoms have been marked in the images with crosses and the chlorines with squares.

effect in delocalized molecular orbitals in the case of nonresonant inelastic tunneling. In the first part, we demonstrate how a local vibrational perturbation is seen in the local electronic structure of the molecule. In the second part, we create spatial IETS maps and interpret them in light of the spectra. In addition, we test how the electronic structure of different substrates tends to distort the IETS map and what consequences this has on detecting the carrier wave effect.

For the IETS maps, the most interesting bias voltages correspond to the $\pm\hbar\Omega_q$ edges of the self-energy. Hence, we calculate the STS and IETS maps at the energies corresponding to the chosen vibrational modes—−50 and 50 mV for CB and −48 and 48 mV for MDCB. For a basic model of a substrate, we use a 5 eV Lorentz LDOS with zero mean, and the other parameter sets (see Sec. III B) are used to probe the robustness of the carrier wave effect. Despite the wide choice of substrate parameters we will not enter a more detailed analysis of the substrate effect on the STS spectra and maps. Instead, we just show a representative example of an STS map for both molecules in the case of a wide-band substrate.

In order to see the IETS maps in contrast with the local density of states, in Fig. 5 we show the calculated constant height STS maps for both molecules at their negative vibrational energies. Here we utilize the wide-band substrate model. There is, in fact, very little variation in the dI/dV mappings of either molecule with different substrates or bias voltages. For CB the benzene appears quite ringlike, with the carbons next to the chlorine-bonded carbon appearing most pronounced in the images. The chlorine can be seen as a separate protrusion from the benzene ring. In the case of MDCB the benzene appears trianglelike, with the carbons next to the substituted ones most visible. Once again, the chlorines are seen distinctly separate from the benzene ring. However, one should remember that these are idealized simulated STM images with an infinitely sharp tip, with accuracy not experimentally accessible.

We use diagonal elements of the orbitalwise partial spectrum of Eq. (23) to model the IETS spectrum at the position of the atom corresponding to the chosen orbital. These atom-specific IETS spectra for MDCB and CB are shown on the left of Figs. 6 and 7, respectively, together with the corresponding color codes on the right. Here the substrate is modeled using a relatively wide Lorentz LDOS distribution, with

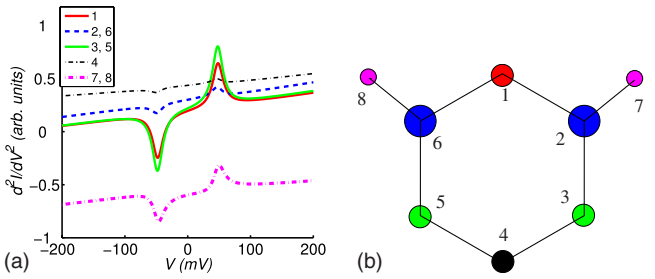

FIG. 6. (Color online) (Left) d^2I/dV^2 spectrum for each atomic p_z orbital contributing to the frontier molecular orbitals of MDCB. (Right) The numbering and color coding used for the atoms in MDCB.

a width of 5 eV centered around the Fermi energy.

While the electron-vibration coupling only creates a nonremarkable kink to the dI/dV spectrum, the effect on its derivative is much more obvious. The general shape of our calculated spectra is very much like those from typical IETS experiments, such as Ref. 7. Here we can see an antisymmetric pair of peaks at positive and negative vibration energies indicating the opening of inelastic tunneling channels above the positive and below the negative bias voltage.

A general feature in these IETS spectra is that the local spectrum at the Cl atoms seems to be shifted toward negative values. The explanation for this is that the onsite energies of p_z orbitals of Cl atoms lie considerably below those of C atoms. Hence, they strongly contribute to the occupied molecular orbitals below the gap but virtually not at all to the unoccupied states above it. This means that the corresponding matrix elements of the local density of states have a decreasing tail for increasing energies within the gap. Consequently, this creates a local negative background to the IETS spectrum.

Thanks to the strong orientation of the p_z orbitals of the constituent atoms of the molecule, these spectra will bring up the most salient features expected to be observed in the IETS maps. Interestingly, while the chosen vibrational modes are directly coupled only to the two Cl atoms (7,8) and the adjoining C atoms (2,6), the vibrational peaks in the *electronic structure* are strongest at C atoms 1, 3, and 5. The IETS signal is moderate on top of the chlorines but on top of the adjoining C atoms (2,6) it almost vanishes. This clearly demonstrates the "carrier wave" effect, where the perturbation in the electronic structure is not necessarily strongest at the site of the vibration. Rather, it is the mutual contribution of the atomic orbitals to the same frontier orbitals that seems to determine the appearance of a strong signal at a chosen orbital.

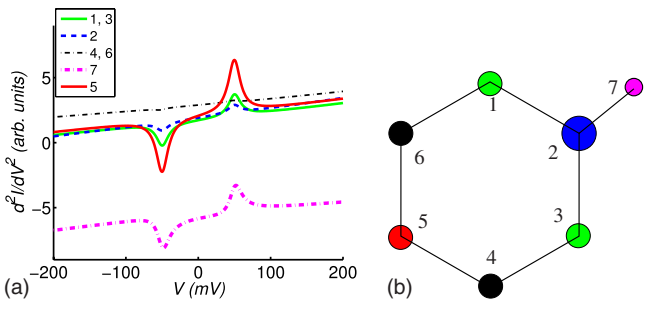

FIG. 7. (Color online) (Left) d^2I/dV^2 spectrum for each atomic p_z orbital contributing to the frontier molecular orbitals of CB. (Right) The numbering and color coding used for the atoms in CB.

The same general trend is seen in the simulated partial d^2I/dV^2 spectra of the CB orbitals as shown on the left of Fig. 7(a) (see accompanying color code on the right). Again, the shape of the simulated spectra corresponds nicely to those generally obtained in experiments. For CB, the difference between the position of the electron-vibration coupling and the site of a strong IETS signal is even more drastic. The intensity is highest at C atom 5, at the end of the molecule opposite to the chlorine, and it is also moderately strong at the chlorine and carbons 1 and 3. At the carbon adjoining the chlorine, the signal is again very weak.

Calculation of the IETS spectra for narrow-band substrates and bands with the edge near Fermi energy create a much more complex pattern. In such a case, the molecule-substrate coupling creates new states to the gap, hence increasing the proportion of resonant tunneling through the molecule. Obviously, the carrier wave effect is still present but the substrate gets mixed to the background of the IETS spectrum in a subtle way, and hence predicting "brightest" and "darkest" orbitals requires a detailed modeling of the substrate. Nevertheless, the calculations with 5 and 10 eV bands centered around the Fermi energy—both for constant density and Lorentzian—show that the absence of strong variations in the substrate electronic structure help retain the general pattern of the spectrum.

The features of the IETS spectra also anticipate the features of the IETS maps at different bias voltages. In the case of moderately varying substrate states, the Cl atoms should distinguish themselves as particularly dark structures at the negative vibrational energy while the C atoms strongly coupled to the electron-vibration perturbation should appear particularly bright at the positive vibration energy. However, for narrow structured bands, the shifting of the background would make the structure of the maps much less predictable.

Figure 8 shows a set of IETS maps at negative voltages. The maps of the top row are those of CB molecules on two different substrates. The top left one is calculated for a 5 eV Lorentz substrate centered around the Fermi energy. As expected, the signal is strong (negative) at the location of the chlorine, and practically no signal at all comes through atoms 4 and 6. Carbons 1 and 3 and carbon 5 are rather clearly seen, which also is in accord with the spectrum of Fig. 7. The relatively high contrast of the carbon adjoining the chlorine is mainly due to a constructive interference between the signals through atoms 1 and 3. This particular case is a very clear demonstration of the carrier wave effect, where the signal is seen at the opposite end of the molecule from the position of the electron-vibration coupling. Furthermore, this pattern very much resembles the HOMO of CB molecule (see Fig. 1) since this is virtually the only FO, to which the orbitals of Cl contribute.

This behavior breaks down at the narrow-band limit with a 1 eV Lorentz LDOS. Figure 8 (top right) shows a representative example of an IETS map in the case where the center of the surface state is within a range from the Fermi

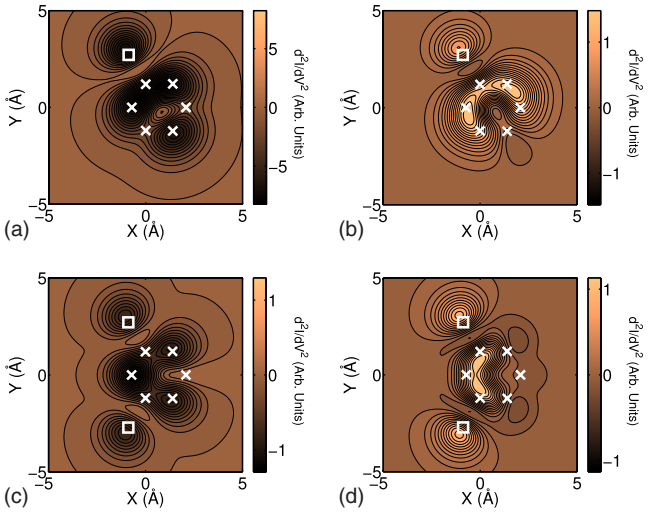

FIG. 8. (Color online) Constant height mappings of d^2I/dV^2 at 2 Å above the plane of the CB and MDCB molecules at negative bias voltages (−48 mV for MDCB and −50 mV for CB). The CB images (top row) have been calculated with Lorentz substrates of widths 5 eV (top left) and 1 eV (top right). The MDCB images (bottom row) have been calculated with Lorentz substrates of widths of 5 eV (bottom left) and 1 eV (bottom right). In all images the substrate LDOS is centered around the Fermi energy. The carbon atoms have been marked with crosses and the chlorines with squares.

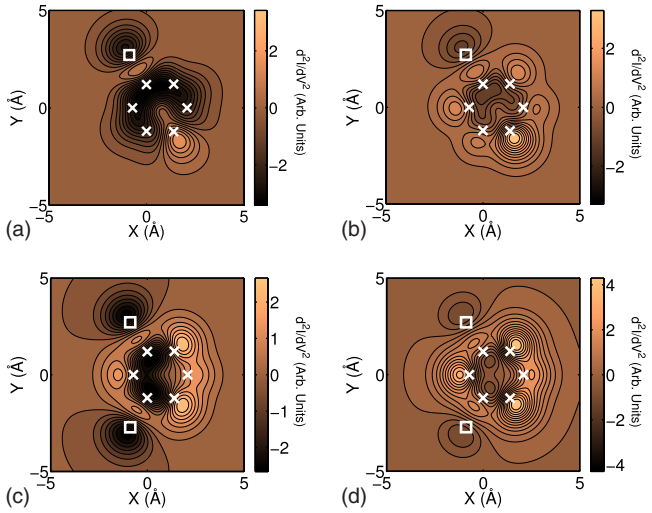

FIG. 9. (Color online) Constant height mappings of d^2I/dV^2 at 2 Å above the plane of the CB and MDCB molecules at positive bias voltages (48 mV for MDCB and 50 mV for CB). The CB images (top row) have been calculated with Lorentz substrates of width 5 eV, centered around the Fermi energy (top left) and at 2.5 eV (top right). The MDCB images (bottom row) have been calculated with Lorentz substrates of width 5 eV, centered around the Fermi energy (bottom left) and at 2.5 eV (bottom right). The carbon atoms have been marked in the images with crosses and the chlorines with squares.

energy to the neighborhood of the LUMO levels. Most dramatically, the sign of the d^2I/dV^2 is positive everywhere, except at atom 5, where it is essentially zero. Evidently, the substrate induces states at around Fermi energy, which tends to favor increasing LDOS at negative energies, creating a (strongly atomic-orbital-dependent) positive background. This is a striking counter example of a case where it is not sufficient to consider merely the electron-vibration coupling and mutual contribution of atomic orbitals to frontier orbitals.

As in the case of CB at negative voltages, MDCB is also rather robust to band width and position at the wide-band limit with negative bias voltages. In Fig. 8 (bottom left) we can see an example, which is very consistent with the spectrum in Fig. 6. Here the signal is clearly strongest at carbon 1, with moderate signal strengths at carbons 3 and 5 and at the chlorines. This demonstrates—even more clearly than CB—how the contrast of the IETS signal is strongly related to the electronic structure of the molecule if the substrate effect is weak. In this case, however, there exists no straightforward relation to the pattern of molecular orbitals since for MDCB, the p_z orbitals of chlorine atoms contribute to all the FOs. The contribution to both of the occupied FOs is especially strong.

The mapping changes noticeably in the case of a 1 eV Lorentz LDOS with the mean at either the Fermi energy or close to the LUMO states. An example is shown in Fig. 8 (bottom right). The IETS signal at carbons 3 and 5 vanishes almost completely but now the signal is most strongly visible around carbons 1, 2, and 6. Again, the derivative of the signal also changes, with the same reasons as for the CB molecule. These effects are thus very similar to the case of CB, showing how substrates with peaked LDOS features very strongly distort the IETS map of the adsorbed molecule.

At positive bias voltages, even the wide-band d^2I/dV^2 mappings become more sensitive to the width and the position of the substrate band, although the general features remain more or less the same in switching between constant LDOS and Lorentz band. It is notable that according to the spectra with a wide-band substrate, the local signal of chlorine atoms remains negative also at positive voltages, which seems to exist even at the narrow-band case.

The IETS map of CB in the case of a 5 eV Lorentz distribution centered around the Fermi energy is shown in Fig. 9 (top left). The carbon atom at the end opposite to chlorine seems to be clearly distinguishable from the rest of the molecule, which is rather expected by considering the IETS spectrum for the molecule. We also see a very clear carrier wave effect. It is also notable that almost the rest of the molecule gives a negative signal. The only exception is the carbon adjoined to the Cl.

The most drastic difference with a wider LDOS can be found when a Lorentz 5 eV distribution is centered around the LUMO states, as seen in Fig. 9 (top right). Here the relative strengths of the positive areas have grown to engulf the negative area completely. The signal is now strongly visible only at carbon 5, at the opposite end of the molecule from the location of the actual vibration. On the other hand, shifting the substrate states toward higher energies also seems to cause an almost constant positive shift of the local d^2I/dV^2.

For MDCB, the mappings with positive bias voltages are somewhat more stable at the wide-band limit than for CB.

Figure 9 (bottom left) shows a mapping of the IETS spectra of MDCB with a 5 eV Lorentz LDOS centered around the Fermi energy. The spectrum of Fig. 6 would anticipate strong negative contrast at the chlorines, which is also the case here. In addition, carbons 3 and 5 should give a strong positive contrast, as well as carbon 1—this is clearly the case in the map. Notably, there seems to be a slightly constructive interference between carbons 3 and 5 at positive energies, and hence the bright pattern is extended to carbon 4, which itself should give a weak signal. On the other hand, a destructive interference seems to invert the contrast of the inside of the molecule.

As the center of the substrate band is shifted from the Fermi energy to the energy of the LUMO level, the mapping once again changes, although less drastically. Figure 9 (bottom right), shows a mapping for a 5 eV Lorentz LDOS centered around the LUMO states. Also in this case, shifting the substrate band toward higher energies generally tends to shift the local IETS signal to a positive direction. This emphasizes the signal from carbons 1, 3, and 5. On the other hand, the signal is once again very weak at the actual location of the vibration itself.

With 1 eV wide distributions the IETS mappings at positive bias voltages get totally erratic, varying greatly with the shape and centering of the LDOS of the substrate. On substrates with peaked LDOS properties, the visibility of the IETS signal at different positions greatly depends on the structure of the substrate, and accurate modeling of the substrate is essential.

V. CONCLUSIONS

In this paper, we have derived Green's-function-based instruments for analyzing IETS-STM experiments. We have also shown, how the effect of the substrate can, in a rather general form, be modeled as a self-energy matrix of the adsorbed molecule. A more fundamental theoretical result here is to derive consistent expressions for the elastic and inelastic effects of the electron-vibration coupling to the electronic Green's function both in the atomic-orbital basis and in the real-space displacement basis of the molecular vibrations. The benefit of this real-space decomposition is that we can separately consider a mechanical perturbation to a certain bond and its effects on the electronic structure at any chosen position.

From a physical point of view, we find a carrier wave effect, where the electronic structure can transfer the effect of a local electron-vibration coupling spatially quite far away within the molecule. We emphasize that the vibration itself is not transferred anywhere but its effect on the electronic structure is as delocalized as the molecular orbitals to which the vibration is coupled.

Considering a few model examples, we show that the carrier wave effect can be distinguished from the IETS experiments in the case of a substrate with little structure around the Fermi energy. In case of a strongly structured substrate the electronic states, which are additionally induced within the energy gap, make it difficult to separate different ingredients of the IETS pattern. A practical application of the present analysis is that combining standard topographic STM mapping with IETS mapping could help in determining the orientation of the adsorbed molecule. The derived formalism also gives an insight to reversed situations, such as how the STM tip should be positioned so that the STM tunneling current would excite vibrational modes most efficiently, which may be relevant information, e.g., in tip-induced tautomerization or isomerization.[33,34] Therefore, this formalism also describes the causal connection between an electronic perturbation and a subsequent mechanical response.

ACKNOWLEDGMENTS

We are grateful to Karina Morgenstern and Heiko Gawronski for inspiring discussions and hospitality in Hannover. We also would like to thank Sami Paavilainen for valuable discussions. Antti Korventausta would also like to thank the Finnish National Graduate School on Materials Physics and Satakunnan Korkean Teknologian Säätiö for funding.

APPENDIX: ELECTRON-VIBRATION COUPLING IN TIGHT-BINDING BASIS

In the following, we consider the electron-vibration self-energy explicitly in tight-binding basis for electrons and atomic displacement basis for molecular vibrations. Apart from the used basis, the results are rather commonly used but the motivation here is to emphasize how they should appear in this kind of local basis. There are many subtleties concerning many-body and nonequilibrium effects related to electron-vibration coupling, which are not discussed here in full detail, and we refer to more advanced treatises about the topic, e.g., Refs. 19, 20, and 37. The present problem concerns nonresonant tunneling at low voltages, which keeps the problem close to equilibrium; in addition the low density of electron states at the relevant voltages also implies relatively weak electron-vibration coupling, which makes use of free vibrations well grounded.

We assume the set of equilibrium positions $\{R_I\}$ and displacements $\{u_I\}$ for the ions so that the index I contains the index of an atom combined to the x, y, and z components of the position/displacement vector. We utilize the canonical transformation from the displacement u_I to the generalized coordinates Q_q,

$$\begin{cases} Q_q = \langle q|I\rangle u_I \sqrt{m_I} = \sqrt{\dfrac{\hbar}{2\Omega_q}}(a_q + a_{-q}^\dagger) \\ P_q = \langle q|I\rangle \dfrac{p_I}{\sqrt{m_I}} = i\sqrt{\dfrac{\hbar\Omega_q}{2}}(a_q^\dagger - a_{-q}), \end{cases} \tag{A1}$$

where we also introduce the standard second quantization (for a general reference see Ref. 35). $a_q(a_q^\dagger)$ is the annihilation (creation) operator of the phonon of the mode q and Ω_q is the frequency of the mode. $\langle I|q\rangle$ is the projection of the vibrational eigenstate q onto the direction I, Q_q is the corresponding generalized coordinate, and m_I is the mass of the atom under consideration. Note also the Einstein summation over I.

This allows us to couple the vibrational Hamiltonian to the electronic Hamiltonian, where the displacement of ions can be taken into account to the first order,

$$H' \approx H_{\alpha\delta}(\{R_I\})c_\alpha^\dagger c_\delta + \frac{\partial V_{\alpha\delta}}{\partial R_I} u_I c_\alpha^\dagger c_\delta, \tag{A2}$$

where $V_{\alpha\delta}$ is the hopping integral between orbitals α and δ. Hence, the total Hamiltonian is of the form

$$H = V_{\alpha\beta}c_\alpha^\dagger c_\beta + M_I^{\alpha\delta}\langle I|q\rangle Q_q c_\alpha^\dagger c_\delta + \frac{1}{2}P_{-q}P_q + \frac{\Omega_q^2}{2}Q_{-q}Q_q, \tag{A3}$$

where $c_\alpha^\dagger(c_\beta)$ is the creation (annihilation) operator for an electron at site α (β), $M_I^{\alpha\delta}=\frac{1}{\sqrt{m_I}}\frac{\partial V_{\alpha\delta}}{\partial R_I}$ and we use the convention $Q_q^*=Q_{-q}$ and $P_q^*=P_{-q}$.

The corresponding equations of motion for the operators are the following:

$$\begin{cases} i\hbar\dot{c}_\alpha = V_{\alpha\beta}c_\beta + M_I^{\alpha\delta}\langle I|q\rangle Q_q c_\delta \\ \dot{P}_q = -\Omega_q^2 Q_{-q} - M_J^{\gamma\beta}\langle J|q\rangle c_\gamma^\dagger c_\beta \\ \dot{Q}_q = P_{-q}, \end{cases} \tag{A4}$$

where the two latter can be combined,

$$\ddot{Q}_q + \Omega_q^2 Q_q = -M_J^{\gamma\beta}\langle q|J\rangle c_\gamma^\dagger c_\beta. \tag{A5}$$

For the inhomogenous equation Eq. (A5), a special solution, i.e., the fluctuation from the equilibrium value of $Q_q(t)=Q_q^0=0$, can be obtained using the kernel function $K_q(\tau)$ where $\tau=t-t'$,

$$Q_q^{sp}(t) = -M_J^{\gamma\beta}\langle q|J\rangle \int K_q(t-t')c_\gamma^\dagger(t')c_\beta(t')dt' \tag{A6}$$

with a kernel

$$K_q(t-t') = \begin{cases} \frac{i}{\hbar}Q_q(t)Q_q^*(t'), & t > t' \\ \frac{i}{\hbar}Q_q^*(t')Q_q(t), & t' > t \end{cases} \tag{A7}$$

from the Green's function equation for Eq. (A5), where the kernel includes the vibration operators. In constructing an effective electron-electron vibration mediated interaction, the operator form of the kernel is conventionally replaced by its expectation value

$$\begin{aligned} D_q^>(\tau) &= \frac{i}{\hbar}\langle Q_q(t)Q_q^*(t')\rangle, \quad t > t' \\ D_q^<(\tau) &= \frac{i}{\hbar}\langle Q_q^*(t')Q_q(t)\rangle, \quad t' > t, \end{aligned} \tag{A8}$$

which defines the Green's function $D^{\lessgtr}(\tau)$ for interacting vibrations (Note that we mainly follow the $D^{\lessgtr}$ and $G^{\lessgtr}$ notation of, e.g., Ref. 36 appropriate to nonequilibrium Keldysh Green's functions, although the aim is at deriving self-energy terms for a retarded equilibrium Green's function).

After replacing $K_q(\tau)$ with $D_q^{\lessgtr}(\tau)$ in Eq. (A6) and inserting the latter to the electron-vibration term of Eq. (A3), an effective phonon mediated electron-electron coupling is introduced,

$$H^{e-v} = -\lambda \int D_{IJ}(\tau)c_\alpha^\dagger(t)c_\delta(t)c_\gamma^\dagger(t')c_\beta(t')dt' \tag{A9}$$

with $D_{IJ}=\langle I|q\rangle D_q\langle q|J\rangle$ for a renormalized vibration Green's function in local basis.

In the many-body framework, the integrand of the electron-electron interaction term Eq. (A9) can be expanded to a series of Feynman diagrams. In self-consistent Born approximation, only the term

$$\lambda D_{IJ}(\tau)c_\alpha^\dagger(t)c_\beta(t')\langle c_\delta(t)c_\gamma^\dagger(t')\rangle$$

is considered[20,36] since the Hartree term with single time Green's functions is found to make a only small shift to the Hamiltonian. On further elaboration of Eq. (A9), we apply the interacting Green's function for electrons,

$$\begin{aligned} G_{\delta\gamma}^>(\tau) &= -\frac{i}{\hbar}\langle c_\delta(t)c_\gamma^\dagger(t')\rangle, \quad t > t' \\ G_{\delta\gamma}^<(\tau) &= \frac{i}{\hbar}\langle c_\gamma^\dagger(t')c_\delta(t)\rangle, \quad t' > t \end{aligned} \tag{A10}$$

and we end up to a one-electron self-energy term

$$\Sigma_{\alpha\beta}^{e-v}(\tau) = \frac{\hbar}{i}\lambda\langle I|q\rangle[D_q^>(\tau)G_{\delta\gamma}^>\Theta(\tau) + D_q^<(\tau)G_{\delta\gamma}^<(\tau)\Theta(-\tau)] \times\langle q|J\rangle. \tag{A11}$$

It should be notified here that both the vibration and electron Green's functions are renormalized, i.e., they should be self-consistently calculated for the interacting system. However, in many cases (see, e.g., Refs. 20 and 37), a weak electron-vibration coupling is assumed to justify the usage of the Green's function for noninteracting vibrations.

We start discussing the Green's function $D^{\lessgtr}$ from free vibration Green's functions, $D^{0\lessgtr}$. If we apply the transformation of Eq. (A1) and take the thermal average of the occupation numbers, the vibration Green's function turns out to be

$$D_q^{0\lessgtr}(\tau) = \frac{i}{2\Omega_q}[(1+n_q)e^{\mp i\Omega_q\tau} + n_q e^{\pm i\Omega_q\tau}] = i\int \frac{1}{2\Omega}\{[1 + n(\Omega)]e^{\mp i\Omega\tau} + n(\Omega)e^{\pm i\Omega\tau}\}\delta(\Omega-\Omega_q)d\Omega. \tag{A12}$$

Hence in the atomic coordinate basis

$$D_{IJ}^{0\lessgtr}(\tau) = i\int \frac{g_{IJ}^0(\Omega)}{2\Omega}\{[1+n(\Omega)]e^{\mp i\Omega\tau} + n(\Omega)e^{\pm i\Omega\tau}\}d\Omega \tag{A13}$$

with the (vibrational) density-of-states matrix

$$g_{IJ}^0(\Omega) = \langle I|q\rangle\delta(\Omega-\Omega_q)\langle q|J\rangle. \tag{A14}$$

The obtained free vibration Green's function can, in principle, be converted into the renormalized vibration Green's function using Dyson's equation

$$D = D^0 + D^0 \Pi D, \tag{A15}$$

where Π is the susceptibility term calculated from electron and hole Green's functions (see, e.g., Ref. 19). From this equilibrium Green's function one could extract the renormalized density of states $g(\Omega)$ and utilize Eq. (A13) again, in order to approximate the renormalized kinetic Green's function $D^{\lessgtr}$.

Assuming we have obtained the renormalized Green's functions for both the electrons and vibrations, it is straightforward to write an equation for the "greater" self-energy,

$$\Sigma^{>}_{\alpha\beta}(\tau) = \hbar\lambda \int \frac{g_{IJ}(\Omega)}{2\Omega} \{[1+n(\Omega)]e^{-i/\hbar(\hbar\Omega+E')\tau} + n(\Omega)e^{i/\hbar(\hbar\Omega-E')\tau}\} G^{>}_{\delta\gamma}(E')\, d\Omega dE', \tag{A16}$$

where according to fluctuation-dissipation theorem (which couples equilibrium Green's function to the kinetic Green's function),[19] $-\frac{i}{\hbar}G^{>}_{\delta\gamma}(E) = [1-f(E)]\rho_{\delta\gamma}(E)$ [and $\frac{i}{\hbar}G^{<}_{\delta\gamma}(E) = f(E)\rho_{\delta\gamma}(E)$] with the density matrix $\rho_{\delta\gamma}(E') = \langle\delta|k\rangle\delta(E'-E_k)\langle k|\gamma\rangle$ and the Einstein summation over k. The density matrix, in general, is that of the interacting system.

Let us Fourier transform this for $\tau > 0$ with a positive convergence parameter η,

$$\Sigma^{>}_{\alpha\beta}(E) = -i\lambda \int\int \frac{g_{IJ}(\Omega)}{2\Omega} G^{>}_{\delta\gamma}(E') \times \left[\frac{1+n(\Omega)}{E-\hbar\Omega-E'+i\eta} + \frac{n(\Omega)}{E+\hbar\Omega-E'+i\eta}\right] d\Omega dE'. \tag{A17}$$

Let us make a change in variables $E'' = E' + \hbar\Omega$ to the first part of Eq. (A17) and $E'' = E' - \hbar\Omega$ to the second. This makes the convolution more visible,

$$\Sigma^{>}_{\alpha\beta}(E) = \int dE'' \frac{-i\lambda}{E-E''+i\eta} \int \frac{g_{IJ}(\Omega)}{2\Omega} \{[1+n(\Omega)] \times G^{>}_{\delta\gamma}(E''-\hbar\Omega) + n(\Omega)G^{>}_{\delta\gamma}(E''+\hbar\Omega)\} d\Omega. \tag{A18}$$

Comparing this to the equation of the Hilbert transformation, the imaginary part of the greater self-energy can be extracted,

$$\Gamma^{>}_{\alpha\beta}(E) = \pi\lambda \int \frac{g_{IJ}(\Omega)}{2\Omega} \{[1+n(\Omega)]G^{>}_{\delta\gamma}(E-\hbar\Omega) + n(\Omega)G^{>}_{\delta\gamma}(E+\hbar\Omega)\} d\Omega, \tag{A19}$$

where $\Gamma^{>}(E) = -i[1-f(E)]\Im[\Sigma(E)]$.

The same procedure can be applied to the advanced part and the result for the imaginary part is

$$\Gamma^{<}_{\alpha\beta}(E) = \pi\lambda \int \frac{g_{IJ}(\Omega)}{2\Omega} \{[1+n(\Omega)]G^{<}_{\delta\gamma}(E-\hbar\Omega) + n(\Omega)G^{<}_{\delta\gamma}(E+\hbar\Omega)\} d\Omega \tag{A20}$$

with $\Gamma^{<}(E) = if(E)\Im[\Sigma(E)]$.

Combining these two we get the imaginary part of the total electron-vibration self-energy

$$\Im[\Sigma^{e-v}_{\alpha\beta}(E)] = -\pi\hbar\lambda \int \frac{g_{IJ}(\Omega)}{2\Omega} [G^{\gtrless}_{\delta\gamma}(E-\hbar\Omega) + G^{\lessgtr}_{\delta\gamma}(E+\hbar\Omega)] d\Omega \tag{A21}$$

with $-\frac{i}{\hbar}G^{\gtrless}_{\delta\gamma}(E) = [1+n(\Omega)-f(E)]\rho_{\delta\gamma}(E)$ with and $-\frac{i}{\hbar}G^{\lessgtr}_{\delta\gamma}(E) = [n(\Omega)+f(E)]\rho_{\delta\gamma}(E)$.

The total self-energy is then obtained by the Hilbert transformation: hence, the coupling Hamiltonian can be embedded into the electronic Hamiltonian as an energy dependent self-energy. The last steps of the previous derivation are parallel to the arguments of Refs. 15 and 36–38 but the result is shown in a different basis.

In this work we assume that $f(E) = f^0(E)$ and $n(\Omega) = n^0(\Omega)$, i.e., the nonequilibrium occupation density does not deviate from the equilibrium statistics. Furthermore, we use the limit of $T=0$ and thus Eq. (A21) is approximated by

$$\Im[\Sigma^{e-v}_{\alpha\beta}(E)] \approx -\pi\hbar\lambda \int \frac{g_{IJ}(\Omega)}{2\Omega} [\Theta(E-\hbar\Omega)\rho_{\delta\gamma}(E-\hbar\Omega) + \Theta(-E-\hbar\Omega)\rho_{\delta\gamma}(E+\hbar\Omega)] d\Omega, \tag{A22}$$

where the zero level of energy has been set to local chemical potential, which at the equilibrium limit is equal to the Fermi energy of the substrate. Hence, the imaginary part is proportional to the convolution of the density of states of vibrations with the occupied and unoccupied electronic states separately. This formula is very handy in deriving generic forms of self-energy using a certain typical form of electronic and vibrational spectra. This is a rather standard way to approximate the electron-vibration coupling in photoemission spectroscopy at low temperatures.[21]

To demonstrate, how Eq. (A22) is used, we show the generic result for Einstein model for vibrational density of states, $g_{IJ}(\Omega) = \delta(\Omega-\Omega_q)$, and a constant electronic density of states, $\rho_{\delta\gamma}(E) = \rho$. The convolution of Eq. (A22) is readily seen to be

$$\Im[\Sigma^{e-v}_{\alpha\beta}(E)] \approx -\rho\frac{\pi\hbar\lambda}{2\Omega_q}[\Theta(E-\hbar\Omega_q) + \Theta(-E-\hbar\Omega_q)]. \tag{A23}$$

This can be transformed into the total self-energy by Hilbert transformation

$$\Sigma^{e-v}_{\alpha\beta}(E) = -\frac{1}{\pi}\lim_{W\to\infty}\int_{-W}^{W} \frac{\Im[\Sigma^{e-v}_{\alpha\beta}(E')]}{E-E'+i\eta} dE' = \rho\frac{\hbar\lambda}{2\Omega_q}\ln\left(\frac{\hbar\Omega_q - E - i\eta}{\hbar\Omega_q + E + i\eta}\right). \tag{A24}$$

This equation falls into the family of generic self-energies which are used to produce the phonon kink to in modeling of electron spectroscopies.[21,39]

*antti.korventausta@tut.fi

[1] B. C. Stipe, M. A. Rezaei, and W. Ho, Science **280**, 1732 (1998).
[2] J. R. Hahn, H. J. Lee, and W. Ho, Phys. Rev. Lett. **85**, 1914 (2000).
[3] M.-L. Bocquet, H. Lesnard, and N. Lorente, Phys. Rev. Lett. **96**, 096101 (2006).
[4] H. Gawronski, M. Mehlhorn, and K. Morgenstern, Science **319**, 930 (2008).
[5] N. Okabayashi, Y. Konda, and T. Komeda, Phys. Rev. Lett. **100**, 217801 (2008).
[6] N. Ogawa, G. Mikaelian, and W. Ho, Phys. Rev. Lett. **98**, 166103 (2007).
[7] H. Gawronski and K. Morgenstern (private communication).
[8] J. Tersoff and D. R. Hamann, Phys. Rev. B **31**, 805 (1985).
[9] B. N. J. Persson and A. Baratoff, Phys. Rev. Lett. **59**, 339 (1987).
[10] N. Lorente and M. Persson, Phys. Rev. Lett. **85**, 2997 (2000).
[11] N. Lorente, M. Persson, L. J. Lauhon, and W. Ho, Phys. Rev. Lett. **86**, 2593 (2001).
[12] T. N. Todorov, G. A. D. Briggs, and A. P. Sutton, J. Phys.: Condens. Matter **5**, 2389 (1993).
[13] J. B. Pendry, A. B. Prêtre, and B. C. H. Krutzen, J. Phys.: Condens. Matter **3**, 4313 (1991).
[14] J. Nieminen, E. Niemi, V. Simic-Milosevic, and K. Morgenstern, Phys. Rev. B **72**, 195421 (2005).
[15] J. Nieminen, I. Suominen, R. S. Markiewicz, H. Lin, and A. Bansil, Phys. Rev. B **80**, 134509 (2009).
[16] P. Sautet, Surf. Sci. **374**, 406 (1997).
[17] Y. Meir and N. S. Wingreen, Phys. Rev. Lett. **68**, 2512 (1992).
[18] J. A. Nieminen and S. Paavilainen, Phys. Rev. B **60**, 2921 (1999).
[19] D. A. Ryndyk, R. Gutierrez, B. Song, and G. Cuniberti, in *Energy Transfer Dynamics in Biomaterial Systems*, edited by I. Burghadt, V. May, D. A. Mischa, and E. R. Bittner (Springer, New York, 2009).
[20] T. Frederiksen, M. Paulsson, M. Brandbyge, and A.-P. Jauho, Phys. Rev. B **75**, 205413 (2007).
[21] F. Reinert and S. Hüfner, in *Photoemission Spectroscopy with Very High Energy Resolution: Studying the Influence of Electronic Correlations on the Millielectronvolt Scale*, edited by S. Hüfner (Springer, New York, 2007).
[22] O. Fischer, M. Kugler, I. Maggio-Aprile, C. Berthod, and C. Renner, Rev. Mod. Phys. **79**, 353 (2007).
[23] W. A. Harrison, *Electronic Structure and the Properties of Solids—The Physics of The Chemical Bond* (Dover, New York, 1989).
[24] We note in passing that also the tip-sample interaction can be written in a contact self-energy form, as well: $\Sigma^L_{s's} = V^\dagger_{s't} G_{tt'}(E_F) V_{t's}$, and hence $\Gamma^L_{s's} = -\frac{1}{\pi}\Im(\Sigma^L_{ss'}) = V^\dagger_{s't}\rho_{tt'}(E_F)V_{t's}$. Applying the same definition to the self-energies related to the sample: $\Gamma^R_\alpha = -\frac{1}{\pi}\Im(\Sigma_{\alpha\alpha'})$, we end up to the form: $\sigma = \frac{2\pi e}{\hbar}\Sigma_{tt'ss'\alpha}\Gamma^L_{s's}G_{s\alpha}\Gamma^R_{\alpha\alpha'}G^-_{\alpha's'}$, which is formally similar to the equation in Ref. 17.
[25] J. P. Perdew, J. A. Chevary, S. H. Vosko, K. A. Jackson, M. R. Pederson, D. J. Singh, and C. Fiolhais, Phys. Rev. B **46**, 6671 (1992).
[26] G. Kresse and J. Hafner, Phys. Rev. B **47**, 558 (1993); **49**, 14251 (1994); G. Kresse and J. Furthmüller, Comput. Mater. Sci. **6**, 15 (1996); Phys. Rev. B **54**, 11169 (1996).
[27] P. E. Blöchl, Phys. Rev. B **50**, 17953 (1994).
[28] G. Kresse and D. Joubert, Phys. Rev. B **59**, 1758 (1999).
[29] V. Simic-Milosevic, J. Meyer, and K. Morgenstern, Phys. Chem. Chem. Phys. **10**, 1916 (2008).
[30] J. Meyer and K. Morgenstern, visualization of vibrational modes for chlorbenzene derivates, http://www.fkp.uni-hannover.de/~morgenstern/chlorobenzene
[31] A. Korventausta, S. Paavilainen, E. Niemi, and J. Nieminen, Surf. Sci. **603**, 437 (2009).
[32] J. C. Slater and G. F. Koster, Phys. Rev. **94**, 1498 (1954).
[33] P. Liljeroth, J. Repp, and G. Meyer, Science **317**, 1203 (2007).
[34] V. Simic-Milosevic, M. Mehlhorn, K.-H. Rieder, J. Meyer, and K. Morgenstern, Phys. Rev. Lett. **98**, 116102 (2007).
[35] C. Kittel, *Quantum Theory of Solids* (Wiley, New York, 1987).
[36] G. D. Mahan, *Many Particle Physics*, 3rd ed. (Kluwer Academic/Plenum Press, New York, 2000).
[37] M. Paulsson, T. Frederiksen, and M. Brandbyge, Phys. Rev. B **72**, 201101(R) (2005).
[38] M. Hengsberger, R. Frésard, D. Purdie, P. Segovia, and Y. Baer, Phys. Rev. B **60**, 10796 (1999).
[39] D. S. Inosov, arXiv:0807.1434 (unpublished).